This document was prepared in conjunction with work accomplished under Contract No. DE-AC09-96SR18500 with the U. S. Department of Energy.

DISCLAIMER

Evaluation of Oxidation and Hydrogen Permeation in Al-Containing Duplex Stainless Steel Alloys

Thad M. Adams*, Paul Korinko, and Andrew Duncan
Savannah River National Laboratory, Aiken SC 29803

oxidation: hydrogen permeation, duplex stainless steels

Abstract

As the National Hydrogen Economy continues to develop and evolve the need for structural materials that can resist hydrogen assisted degradation will become critical. To date austenitic stainless steel materials have been shown to be mildly susceptible to hydrogen attack which results in lower mechanical and fracture strengths. As a result, hydrogen permeation barrier coatings are typically applied to these steel to retard hydrogen ingress. The focal point of the reported work was to evaluate the potential for intentional alloying of commercial 300-series stainless steels to promote hydrogen permeation resistant oxide scales. Previous research on the Cr- and Fe-oxide scales inherent to 300-series stainless steels has proven to be inconsistent in effecting permeation resistance. The approach undertaken in this research was to add aluminum to the 300-series stainless steels in an attempt to promote a pure Al-oxide or and Al-rich oxide scale. Al-oxide had been previously demonstrated to be an effective hydrogen permeation barrier. Results for 304L and 347H alloys doped with Al in concentration from 0.5-3.0 wt% with respect to oxidation kinetic studies, cyclic oxidation and characterization of the oxide scale chemistry are reported herein. Gaseous hydrogen permeation testing of the Al-doped alloys in both the unoxidized and oxidized (600°C, 30mins) conditions are reported. A critical finding from this work is that at concentration as low as 0.5 wt% Al, the Al stabilizes the ferrite phase in these steels thus producing duplex austenitc-ferritic microstructures. As the Al-content increases the amount of measured ferrite increases thus resulting in hydrogen permeabilities more closely resembling ferritic steels.

Introduction

With the resurgence of interest in the development of a national hydrogen economy a considerable increase in scientific exploration concerning hydrogen production and storage has occurred within the last five years. Numerous technologies including biomass production, high temperature electrolysis, thermochemical cycles, advanced gaseous storage tanks, chemical hydrides, and advanced metal hydrides are being developed to provide competitive alternatives to fossil fuel energy technologies. One issue for successful commercial implementation of these technologies is the ability of structural materials for process vessels and piping, storage containers, and engineered components to resist embrittlement from hydrogen.

Hydrogen embrittlement, hydrogen induced cracking, and hydrogen corrosion cracking have long been studied for a wide variety of materials and operating conditions [1-8]. NASA in 1997 performed a comprehensive review of hydrogen compatibility data of various materials as part of a safety analysis. From this review NASA developed a hydrogen materials compatability matrix that identified acceptable and unacceptable materials for hydrogen service environments.

A major structural component material for hydrogen service applications are austenitic stainless steels—304L, 316L,etc. These austenitic stainless steels have been previously shown to have a mild susceptibility to hydrogen embrittlement. However, this susceptibility can vary with changing environmental conditions--temperature, pressure, surface finish—and as such these materials are often coated with permeation barriers to minimize the potential impact from hydrogen exposure. Many permeation barrier coating materials—Al, Al_2O_3, TiC, TiN, W, BN, Ni, Mo, Sn, H_3PO_4 glass, TiO_2, Cr, Cr_2O_3--have been evaluated through the years [9]. These materials have shown permeation reductions that range from 10-10000X during laboratory testing. This variation is due to several factors such as the inherent permeation resistance of the coating material, surface preparation, coating microstructure, and application technique. Of the various permeation barrier materials studied, Al/Al_2O_3 structures have had the most commercial success and implementation—as diffused aluminide coatings-- and have shown permeation reduction factors on the order of 10000+. In previous applications, Al_2O_3 permeation barriers resulted from application techniques used to apply Al-rich coatings [10-12]. Aluminum rich coatings applied by either vapor deposition or packed bed technologies have been shown to possess inherent Al_2O_3 layers at their outermost surface. It has long been perceived that this outer 1-2μ of oxide provides the majority of the permeation resistance for these Al-rich coatings [10]. Additionally, much attention has been given to evaluating the permeation resistance of natively grown oxides on austenitic stainless steel and Ni-base alloys. These oxides primarily consist of Fe_2O_3, Cr_2O_3, or spinel-Cr_2MO_4 (M= Ni, Fe, Co). Of these three surface oxides, Cr_2O_3 has been shown to be the most hydrogen/hydrogen isotope resistant reducing the permeation in some cases by up to 2-3 orders of magnitude [9].

As a result of the previously demonstrated successes of both Al_2O_3 and Cr_2O_3 with respect to hydrogen permeation resistance [13-15], the focal point of this study has been to attempt to develop advanced Fe-Cr-Ni-Mn-Al alloys that form a continuous adherent Al_2O_3 layer or a mixed Al_2O_3- Cr_2O_3 layer to provide permeation resistance with the need for an external coating/coating application technique. This approach has the potential advantage of being amenable to welded components which are often problematic for external coating approaches.

Experimental Approach

Batch heat ingots of approximately 25kgs each were prepared using vacuum induction melting. The base compositions for each ingot were based on conventional 304L and 347H austenitic stainless steel alloy compositions—ASTM A240. Alloying addition of 0.5wt-7.0wt% aluminum, although only alloys up to

*contact author: Thad Adams, SRNL, thad.adams@srnl.doe.gov

3% were subsequently permeation tested, to the base compositions were made and the as-cast ingots were processed via the following working schedule: 1) the 4-in square ingots were hot forged at 1000°C down to 1.5 inches square sections at 0.5-in reduction per pass. The 1.5-in sections were hot-rolled @1000° in multiple passes down to approximately 1-in thick sections. A final thermal treatment of the 1-in sections was performed at 950°C for 1 hour followed by a water quench.

Analysis of the chemical composition of the final 1-in sections was performed for the four heats—typical values for 3wt%Al doped alloys provided in Table 1. Characterization of the as-processed microstructure was performed using light optical microscopy on polished sampled electrolytically etched in a solution of 10% oxalic acid. Scanning electron microscopy and energy dispersive x-ray spectroscopy were performed to characterize the phase structure and chemical analysis. In addition, X-ray diffraction was used to determine the phases present in the alloys.

The ferrite content of the samples was determined using a Fischer Ferrite Scope. The instrument was calibrated and the ferrite content ascertained from the relative magnetic strength of the ferrite.

Oxidation kinetic testing was performed via thermogravimetric analysis in a TA-TGA system operated at 600°C and 1000°C with isothermal holds of 2-hrs at temperature. Additional testing to examine the cyclic oxidation behavior was performed at 1000°C in air for cycles of nominally 24 and 48 hrs with a total exposure time of approximately 1000-hrs. Weight change of the cyclic oxidation samples was measured using a five-place balance.

The evaluation of oxide scale chemistry was performed on samples oxidized at 450°C and 600°C for 2-hrs and 30-mins respectively. Following these oxidation treatment the surface oxide layer chemistry was analyzed via Auger Electron Spectroscopy using a Perkins-Elmer PHI 660 Scanning Auger Mulitprobe.

Preliminary hydrogen permeation testing was conducted at the Savannah River National Laboratory using the permeation test rig shown in Figure X. Tube samples, 19 mm diameter and 0.89 mm thick, were brazed into 2.12" diameter Conflat (CF) flanges. The sample assemblies were placed in a 1" OD vacuum system fabricated with 2.12" CF flanges. Copper gaskets were used to seal the samples. The samples were evacuated to 1 x 10^{-6} Torr for a period of at least six hours at room temperature. The samples were then heated to 100C for 8 to 16 hours to outgas the system. The sample was finally heated to the test temperature of 300C. A leak rate test was conducted. If the leak rate was not linear, the sample was evacuated for additional time, after an acceptable leak rate was obtained, the sample section valves were closed and 400 Torr of deuterium was introduced. It took approximately 2-3 minutes for the pressure to reach the target value. The pressure rise on the low pressure side of the system was monitored. The data were logged at a 30 second interval. The data were reduced to estimate the Diffusivity and Permeability. The data were plotted as a function of time. The data exhibit three distinct regions, the background in-leakage region, a transition region, and a steady state region, nearly linear region. The diffusivity was estimated by calculating the slope and the intercept of the linear region using a least squares method. These two variables were then used to determine the lag time (t), i.e., the time at which the line crossed the Y-axis at zero. Lag time, t, time was used in the equation t = x2 / 6 D, to determine D. The permeability was estimated from the slope of the curve, the expansion volume, the sample area, and the test pressure.

Results and Discussion

Alloy Characterization

Austenitic stainless steel alloys are primarily comprised of a single phase FCC microstructure; however some BCC ferritic phase also occurs in these alloys with the volume fraction being dependent on alloy composition and processing history. Characterization of the as-processed microstructures of 304L and 347H modified with 3.0wt% Al using optical microscopy is shown in Figure 1. Previous work on Fe-Ni-Al alloys has indicated that up to approximately 0.5wt% Al can be dissolved in austenite. From this same study the remaining 2.5wt% Al would be expected to be found in multicomponent intermetallic phases. However, examination of the 3.0wt% Al alloys clearly show a two-phase structure in the arc melted buttons. X-ray diffraction and scanning electron microscopy data for these alloys has indicated a multi-phase microstructure consisting of austenite, ferrite and an Fe-Ni-Cr-Al intermetallic. The Fe-Ni-Cr-Al intermetallic is believed to be occur as $(Fe, Ni, Cr)_3Al$. Energy Dispersive X-ray spectroscopy (EDS) analysis performed in the SEM shows Al in the austenite matrix thereby confirming the solubility of Al in austenite. The ferrite in the microstructure was usually found in the interdendritic areas adjacent to the Al;-containing intermetallic in the arc melted buttons. Examination of the microstructure of the other arc melted button alloys and conventionally cast and forged alloys with Al-concentration up to 7wt% has shown similar features with increasing ferrite content. Analysis of these alloys using a Fischer Ferritescope to provide a measure of total ferrite content (Table 2) has shown that as the Al concentration increases up to 7wt% so does the ferrite content to the point where the dominate phase in the microstructure is ferrite. The stabilization of the ferrite phase can be attributed to the relative size of the Al atoms in comparison with the austenite (FCC) and Ferrite (BCC) structures. Since the Al atom is rather large the openness of the BCC structure allows for easier accommodation and the Al [16]. The resulting duplex(austenite-ferrite) microstructures from the addition of Al is potentially detrimental for hydrogen service applications since ferrite alloys are typically more susceptible to hydrogen embrittlement and increased permeation. However, the focal point of this program is to understand the nature of the oxide formed on these alloys and as such the duplex structure may not be as damaging as when compared to unoxidized materials.

The hardness of the Al-doped 304L and 347H alloys was measured using a Rockwell Hardness tester to evaluate the influence of Al-content. The hardness of the both alloys increased from approximately 45HRA to 70HRA with increasing Al content up to 7wt%. This 35% (25 point) increase is attributed to the increase in ferrite and Al-containing intermetallic phase volume fraction with increasing Al concentration. Hardness data from samples given homogenization treatments at 900°C for times up to 18 hours show only moderate decreases in hardness. For the 3wt% Al-doped 304L alloy the hardness decreased approximately 11% over the 18-hr treatment whereas the for the 3wt% Al-doped 347H the hardness decreased only 7%. These results are indicative of a reasonably stable microstructure, especially since

*contact author: Thad Adams, SRNL, thad.adams@srnl.doe.gov

cold work is the hardening mechanism for conventional austenitic stainless steels, which is required for long-term service applications.

Oxidation Behavior

One of the primary goals in developing these advanced stainless steel alloys is to promote an oxide scale comprised entirely of Al_2O_3 or to promote a mixed Cr_2O_3- Al_2O_3 that will provide a significant reduction in hydrogen permeation when compared to the base alloy. As a result, a critical factor in the development of these alloys is to understand the oxidation behavior (rate) and chemistry. Isothermal TGA analysis of the oxidation kinetics of the 304L and 347H alloys doped with 3wt% Al has been performed. The specific weight change with time for samples tested at approximately 600°C with a 2-hour isothermal hold is shown in Figure 2. The data presented in Figure 2 shows a 30% decrease and a 50% decrease in oxidation rate for the Al-doped 304L and Al-doped 347H alloys when compared to unalloyed specimens. Thus, the added aluminum in these alloys works to reduce the oxidation rate.

Table 1. Measured Compostions for 3wt%Al-doped Alloys

Element	Al-Doped 304L	Al-Doped 347H
Cr	18.21	17.75
Ni	8.63	9.73
Al	3.34	3.15
Mo	0.10	0.10
Si	0.51	0.61
Mn	1.67	1.63
Nb		0.61
P	0.004	0.007
C	0.010	0.035
O	0.0015	0.0010
N	0.058	0.009
S	0.019	0.025
Fe	Balance	Balance

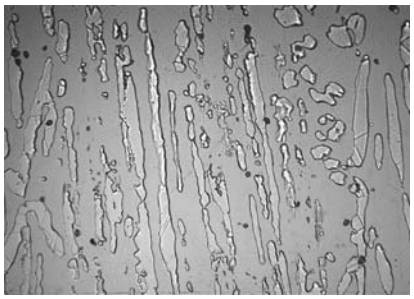

(a)

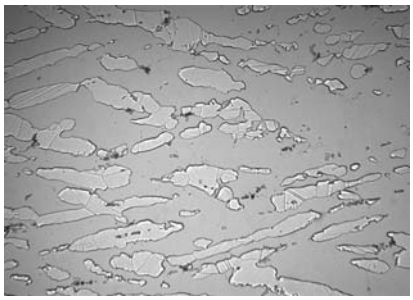

(b)

Figure 1. Typical microstructure of (a) 304L – 3 Al cast and forge (b) 347-3Al cast and forged. Lighter gray dispersoids are ferritic and matrix is austenitic.

Table 2. Measured Ferrite Content for Al-doped Stainless Steel Alloys

Sample ID	Ferrite Content %
304L	0.0
304L	0.7
304L-0.5Al	11.9
304L-1Al	19.3
304L-3Al	61.2
304L-3Al	55.3
304L-3Al	66.0
304L-7Al	84.1
347H	1.0
347H	1.6
347H-0.5Al	8.8
347H-1Al	11.9
347H-3Al	57.9
347H-3Al	49.5
347H-3Al	60.7
347H-7Al	79.8

A further aspect to the oxidation behavior of these Al-doped stainless steel alloys is the cycle oxidation response. Cyclic oxidation of structural alloys has the potential to be the most challenging environment. The stresses generated in the oxide scale and base metal from repetitive heating and cooling cycles often leads to an increase in the rate of spallation as well as the total volume of oxide scale spalled. Spallation of the oxide scale exacerbates the challenge of total materials attack by exposing virgin base material. Cyclic oxidation data collected for specimens tested at 1000°C on a 24hr cycle time for a total of approximately 1000 hrs is provided in Figure 3. The general shape for cyclic oxidation curve data is characterized by an increasing slope to a maximum value followed by an almost linear decreasing slope. Analysis of the data in Figure 3 collected from

*contact author: Thad Adams, SRNL, thad.adams@srnl.doe.gov

the 3wt%Al-doped 304L and 347H alloys shows this characteristic shape. It is interesting to note that for the 3wt% Al-doped 347H alloy greater variability exist in the decreasing linear slope portion of the curve. This indicated greater variability in the oxide scale re-growth-spallation process that occurs once spallation is initiated.

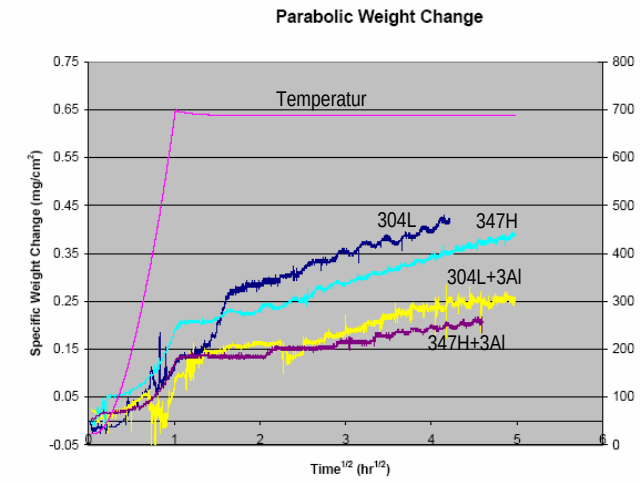

Figure 2. Specific Weight Change for Undoped and Al-doped Stainless Steel Alloys at 700°C in Flowing Air

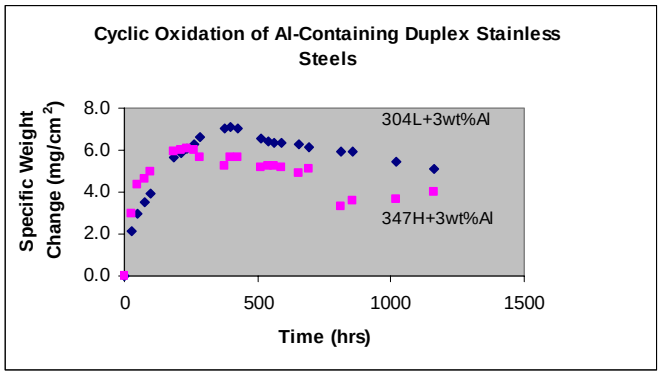

Figure 3. Specific Weight Change for 3 wt% Al-doped Stainless Steel Alloys at 1000°C in Flowing Air

In addition to understanding the oxidation kinetics and scale adherence/spallation behavior, a critical issue in this work has been to characterize the chemical composition of the oxide scale in an attempt to understand how the Al addition affects scale behavior. To approach this question, specimens of the Al-alloyed and unalloyed have been oxidized and the resulting oxide scale chemistry characterized using depth profiling AES. Analysis of the composition of the oxide scales formed on baseline 304L and 347H treated at 600°C for 30 minutes in air is shown in Figure 4. Examination of the AES spectrum collected for both of the undoped baseline alloys shows characteristic oxide scale formation for Fe-Cr-oxidation. Typically Fe-Cr alloys or chromium alloyed steels oxidized at temperatures at or above 600°C develop chromium-rich scales and at temperatures above 900°C they display full chromium-oxide scales [17-18]. The AES spectrum in Figure 4 for both the 304L and 347H samples treated at 600°C for 30 minutes in flowing air show chromium-rich oxide scale with slight chromium depletion and iron enrichment at the near-surface owing to the faster kinetics the chromium oxide growth at this temperature. Results from the AES examination of the oxide scale produced on the Al-doped alloys containing 1wt% or 3wt% Al are provided in Figure 5. These Al-doped samples were also treated at 600°C for 30 minutes in flowing air. The AES spectrum show similar features to the baseline alloys in that the oxide scale are chromium rich however, it is clearly shown that Al enrichment at the surface of these samples occurs for the 3wt% doped alloys and also for the 1wt% doped 347H base alloy. From this data no direct conclusion can be drawn as to the reaction path for the oxide scale formation except that a multicomponent oxide scale forms under the exposure conditions and one of the components of this scale is Al.

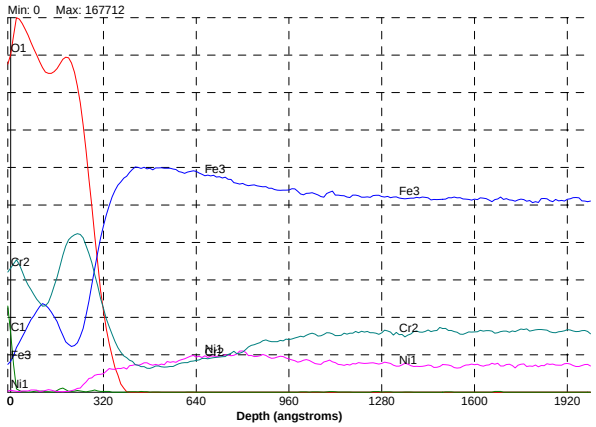

(a)

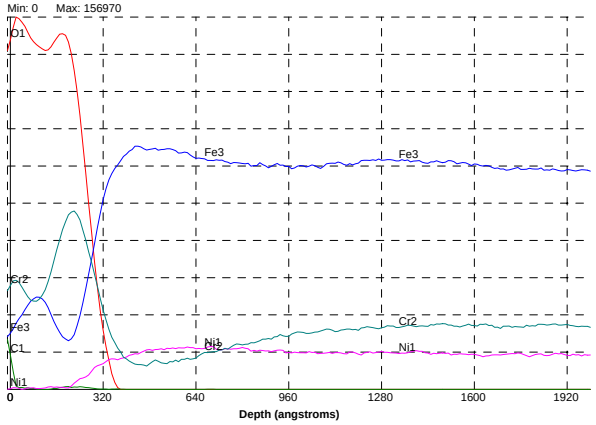

(b)

Figure 4. Auger Analysis of 304L(a) and 347H9b) Alloys Thermally Treated at 600°C for 30 minutes in Air

*contact author: Thad Adams, SRNL, thad.adams@srnl.doe.gov

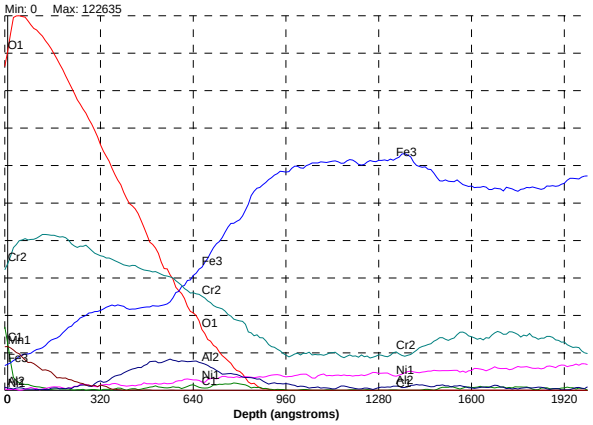

(a)

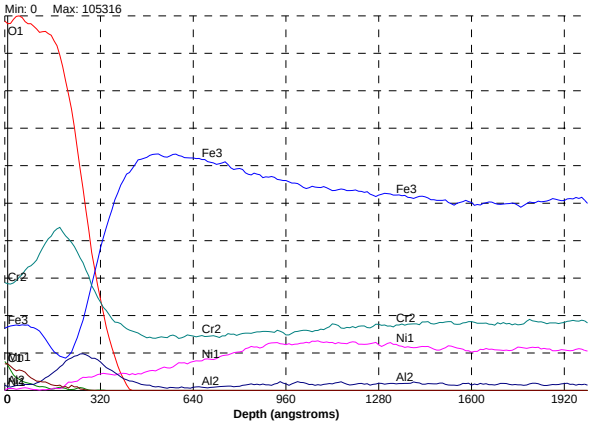

(b)

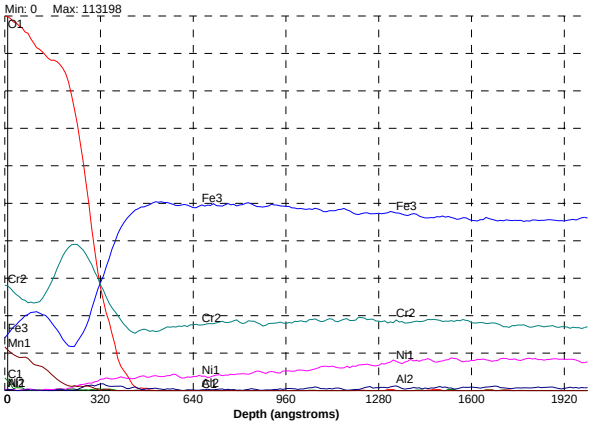

(c)

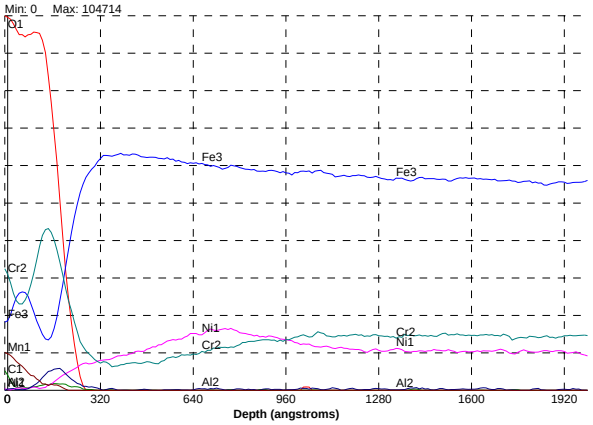

(d)

Figure 5. Auger Analysis of 304L-3Al(a), 347H-3Al(b), 304-1Al(c), and 347H-1Al(d) Alloys Thermally Treated at 600°C for 30 minutes in Air

Hydrogen Permeation

Although understanding the oxidation behavior of these alloys is critica,l the major focus of this research effort was the attempt to tailor these Al-doped alloys for hydrogen service applications. More specifically, the intention for these alloys was to show improved hydrogen permeation resistance. The concern in selecting the compositions was the potential for Al to stabilize the ferrite phase thus producing a duplex microstructure as has already been shown herein. However, even though the baseline microstructure for these alloys is no longer a single phase or mostly single phase austenite, results from the oxidation analysis raise the question of the multi-component mixed oxide scales effectiveness for reducing permeation in these duplex alloy structures.

Hydrogen permeation testing was conducted for baseline un-doped 304L and 347H in both the unoxidized and oxidized conditions (600˚C/1 hour) as well as for the same alloys doped with 3wt% Al in the unoxidized and oxidize conditions. Results from these tests (Figure 6) indicate that the unoxidized Al-doped alloys have the highest permeation rate (Table 3) of all the samples tested. Upon reflection this is not unexpected due to the large fraction of BCC-ferrite present in the microstructure which acts as a high permeation pathway. However, in comparing the unoxidized and oxidized Al-doped alloys the data for the 304L-3Al alloys an order of magnitude decrease is demonstrated for the oxidized versus unoxidized alloy. Examination of the 347H-3Al doped alloy data in the same conditions does not show the same decrease in permeability however, it should be noted that it is suspected that the braze joint used in the sample mounting had failed. What is curious about the behavior of the Al-doped alloys is that in comparing the permeabilities of the baseline alloys, the influence of the surface oxide scales for the undoped alloys seems to have little or no effect on the permeability, i.e., around a factor of 2. From the AES chemistry analyses of the oxide scale in the previous section it is clear that the oxide scale on the undoped alloys are comprised of Fe-and Cr oxides with the innermost layer being Cr-rich while the outer layer being either more Fe-rich or a mixed Fe/Cr-rich layer. This mixed oxide formed at 600°C appears to offer little effect to the transport or dissociation of hydrogen. In comparison, the oxide scale containing Al for the Al doped alloys have shown a significant effect on hydrogen

*contact author: Thad Adams, SRNL, thad.adams@srnl.doe.gov

permeability. It is generally accepted that the additions of elements such as Cr and Al to the oxide scale of steels increases corrosion resistance. It is clear from the AES profiles of the Al-doped steels that the addition of Al during the scale layer formation process influence the overall scale form chemistry and activity of the Fe- and Cr species. The characteristic V-shape concentration profiles for Fe and Cr present in the undoped alloys is replaced by a more constant concentration profile for both Fe and Cr in the scale layers.

Table 3. Hydrogen Diffusivity and Permeation Data

Alloy	***D (cm^2/s)***	***P (atm/s)(cm^4)/($cm^2\sqrt{atm}$)***
304L	8.38E-08	2.14754E-08
304L OX	5.04E-08	1.11252E-08
304l 3Al	3.13E-06	2.20962E-07
304l 3Al OX	6.48E-08	1.3997E-08
347H	1.79E-07	3.07454E-08
347 H Ox	6.18E-08	2.30275E-08
347 H 3 Al	1.14E-06	1.52268E-07
347 H 3 Al Ox	1.13E-05	7.39963E-07

Conclusions

1. The addition of Al to the commercial austenitic stainless steels alloys 304L and 347H results in the stabilization of ferrite producing a duplex ferrite-austenite microstructure—additions as low as 0.5 wt% result in an approximately ten-fold increase in ferrite content. To avoid the ferrite stabilization it would be necessary to reduce the Cr content as the Al content increases.
2. The oxidation kinetics for the Al-doped alloys shows a 1.5-2.0X decrease in the oxidation rate. Cyclic oxidation behavior for these alloys is characteristic displaying an increasing weight gain to a maximum followed by a linear decrease indicative of oxide spallation.
3. Auger Electron Spectroscopy profiles of oxide scale produced from heat treatments of doped and undoped alloys at 600°C for 30 minutes exhibit clear difference in the scale chemistry and near surface elemental distribution. The undoped commercial 304L and 347H alloys display a characteristic mixed-Fe-Cr oxide scale with the innermost layer being more Cr-rich and the outer being more Fe-rich. The alloys doped with 3 wt% Al show in general a more Cr-rich scale thus indicating an affect of the Al on the Cr and Fe activity in the alloy.
4. The hydrogen permeability of the duplex microstructure produced in the Al-doped alloys is higher than the commercial undoped alloy—the diffusivity and permeability values determined are similar to those developed for other duplex stainless steel alloys and for Fe.
5. The Al-containing multicomponent oxide scale formed on the Al-doped alloys has been demonstrated to be effective at reducing the permeation rate than the oxide scale formed on the undoped commercial alloy. The Al-containing scale reduced the permeation rate by an order of magnitude over the unoxidized material to a value comparable to the baseline alloy and condition.

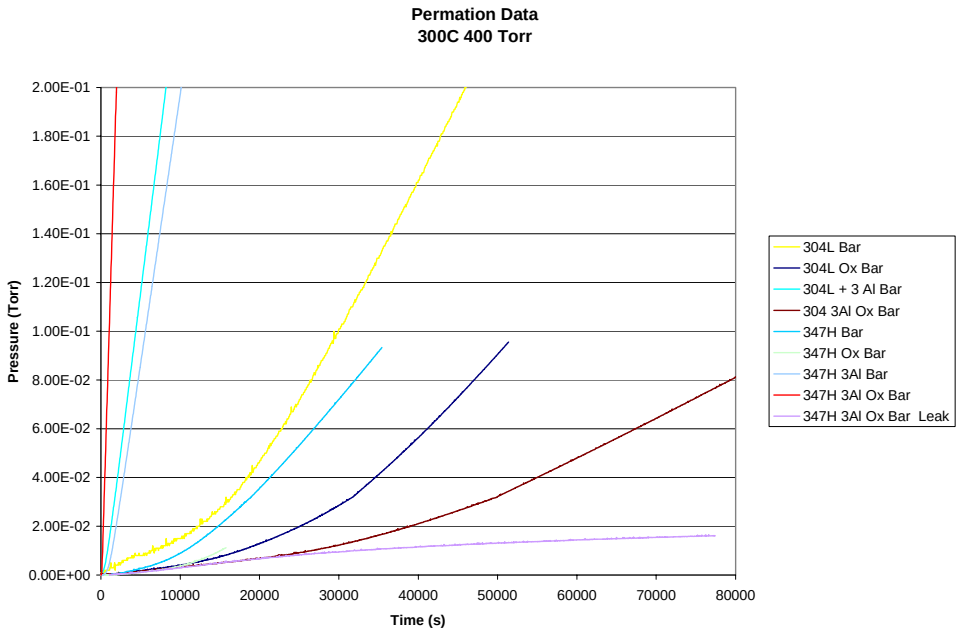

Figure 6. Hydrogen Flux for Undoped and Al-doped 304L and 347H Alloys Measured at 300°C and 400Torr

*contact author: Thad Adams, SRNL, thad.adams@srnl.doe.gov

References

1. H. H. McCoy, Jr. USAEC Report ORNL-3600 June (1964).
2. M. R. Louthan, Jr., in Hydrogen in Metals, ASM, Metals Park, OH, p.53, (1964).
3. M. R. Louthan and A. H. Dexter, Metallurgical Transactions, 6A, 1655, (1975).
4. M. R. Louthan, G. R. Caskey, J. A. Donovan, and D. E. Rawl, Materials Science and Engineering, 10, 357, (1972).
5. M. Mohitpour and H. Solansky, Proceedings of ASME PVP Conference 2004, La Jolla, CA July 2004.
6. K. N. Ankhurst and T. J. Baker, Metallurgical Transactions, **12A**, 1059-1070, (1981).
7. G. Yu, B. Jiang, and L. Qiao, Scripta Materialia, **36,** 1467-1470, 1997.
8. D. Burwell, M. Brongiers, and J. Beavers, Proceedings of ASME PVP Conference 2004, La Jolla, CA, July, 2004.
9. G. W. Hollenberg, E. P. Simonen, G. Kalinin, and A. Terlain, Fusion Engineering and Design **28,** 190-208, (1995).
10. K. Forcey, D. Ross, C. Wu, Journal of Nuclear Materials, **182**, 36-51, (1991).
11. A. Perujo, E. Serra, H. Kolbe, and T. Sample, Journal of Nuclear Materials, **233-237**, 1102-1106, (1996).
12. C. Fazio, K. Stein-Fechner, E. Serra, H, Glasbrenner, and G. Benamati, Journal of Nuclear Materials, **273**, 233-238, (1999).
13. Y. Ishikawa, T. Yoshimura, and M. Arai, Vacuum, **47**(6-8), 701-704, (1996).
14. W. Song, J. Du, Y. Xu, and B. Long, Journal of Nuclear Materials, **246**, 139-143, (1997).
15. Y. Yamada-Takamura, F. Koch, H. Maier, and H. Bolt, Surface Coatings & Technology, **153**, 114-118, (2002).
16. V. Raghavan and D. P. Antia, Metallurgical and Materials Transactions A, **25A**, 2675-2681, (1994).
17. G. Betz, G. Wehner, L. Toth, and A. Joshi, Journal of Applied Physics, **45**, 5312, (1974).
18. G.Hultquist and C. Leygraf, Materials Science and Engineering**, 42**, 199, (1980).

*contact author: Thad Adams, SRNL, thad.adams@srnl.doe.gov